MAUSAM, **77**, 2 (April 2026), 601-612

MAUSAM

DOI: https://doi.org/10.54302/mausam.v77i2.6750
Homepage: https://mausamjournal.imd.gov.in/index.php/MAUSAM

UDC No.551.577.38(594)

A Comparative study of the effects of the Indian ocean dipole and the El Niño in 2019 and 2023 on agricultural drought in Karawang Regency, Indonesia

ACHMAD FAHRUDDIN RAIS[1]*, MEASSA MONIKHA SARI[2], ASMINAR[3*]

[1]*Research Center for Limnology and Water Resources, National Research and Innovation Agency (BRIN), Cibinong, West Java-16911, Indonesia*

[2] *Department of Civil Engineering,Universitas Serang Raya, Serang City, Banten-42162, Indonesia*

[3]*Department of Agribusiness,Universitas Muara Bungo, Bungo, Jambi-37211, Indonesia*

(*Received 17 July 2024, Accepted 19 September 2025*)

***Corresponding author's email: achm050@brin.go.id**

सार – यह अध्ययन 2019 और 2023 में करावांग रीजेंसी के धान के खेतों में सूखे की स्थितियों पर अल नीनो और हिंद महासागर द्विध्रुव (आईओडी) के प्रभावों की जांच करता है। आईओडी और अल नीनो दोनों ही मौसम संबंधी सूखे के माध्यम से कृषि सूखे को अप्रत्यक्ष रूप से प्रभावित करते हैं। 2019 में आईओडी को चरम के रूप में वर्गीकृत किया गया, जबकि 2023 में अल नीनो को मजबूत माना गया । ओशनिक नीनो इंडेक्स (ओएनआई) और द्विध्रुवीय मोड इंडेक्स ने अल नीनो और आईओडी के संकेतकों के रूप में कार्य किया। मानकीकृत वर्षा सूचकांक (एसपीआई) का उपयोग करके मौसम संबंधी सूखे का मूल्यांकन किया गया, जबकि सामान्यीकृत अंतर सूखा सूचकांक (एनडीडीआई) के साथ कृषि सूखे को मापा गया । परिणामों से पता चला कि दोनों वर्षों में सबसे गंभीर सूखे मौसम की स्थिति अगस्त और सितंबर में आई, जिसमें उच्च आईओडी और ओएनआई सूचकांकों के कारण 2023 का सूखा अधिक व्यापक था। इन सूखे और संबंधित आईओडी और अल नीनो घटनाओं के बीच दो महीने की देरी हुई। कृषि सूखे ने 2019 और 2023 के बीच महत्वपूर्ण भिन्नता दिखाई, जिसमें 2019 में उत्तरी और मध्य क्षेत्रों में पहले और अधिक व्यापक सूखा पड़ा, जबकि 2023 में विशिष्ट स्थानों पर बाद में और अधिक तीव्र सूखा पड़ा। यह कृषि सूखा 2019 (2023) में मौसम संबंधी सूखे से लगभग दो (तीन) महीने पीछे था, संभवतः मिट्टी के पानी के प्रतिधारण में अंतर के कारण, जुलाई 2019 (अगस्त 2023) में गिरावट के बाद दोनों वर्षों में अक्टूबर में चरम पर था, जो जलाशय-पोषित सिंचाई से प्रभावित था।

ABSTRACT. This study examines the effects of El Niño and the Indian Ocean Dipole (IOD) in 2019 and 2023 on drought conditions in rice fields in Karawang Regency. Both IOD and El Niño influence agricultural drought indirectly through meteorological drought. The IOD in 2019 was classified as extreme, while the El Niño in 2023 was considered strong. The Oceanic Niño Index (ONI) and Dipole Mode Index served as indicators for El Niño and IOD. Meteorological drought was evaluated using the Standardized Precipitation Index (SPI), while agricultural drought was measured with the Normalized Difference Drought Index (NDDI). The results revealed that the most severe meteorological droughts in both years occurred in August and September, with the 2023 drought being more widespread due to elevated IOD and ONI indices. There was a two-month delay between these droughts and the related IOD and El Niño events. Agricultural drought showed significant variation between 2019 and 2023, with 2019 experiencing an earlier and more extensive drought in the northern and central regions, while 2023 saw a later and more intense drought in specific locations. This agricultural drought lagged behind the meteorological drought by about two (three) months in 2019 (2023), likely due to differences in soil water retention, peaking in October of both years after a decline in July of 2019 (August in 2023) influenced by reservoir-fed irrigation.

Key words – El Niño, Indian ocean dipole, Meteorological drought, Agricultural drought, Standardized precipitation index, Normalized difference drought index.

1. Introduction

Drought is described as a natural phenomenon that occurs temporarily within the climate cycle, with potential widespread impacts on water supply (American Meteorological Society, 2019). It affects both surface water and groundwater resources and can result in reduced water availability, degraded water quality, crop failures, decreased grassland productivity, diminished electricity generation capacity, disruption of riparian habitats, and restrictions on recreational activities (Mishra and Singh, 2010). Wilhite and Glantz (1985) classify drought into four categories based on its effects: meteorological drought causing insufficient rainfall, agricultural drought leading to inadequate water supply for crops and consequent yield reductions, hydrological drought resulting in reduced water levels in rivers, reservoirs, and groundwater, and socio-economic drought affecting the supply and demand of economic goods.

Indonesia is located west of the Pacific Ocean and east of the Indian Ocean, which is directly influenced by these oceanic regions' weather and climate dynamics. Significant natural occurrences affecting Indonesia are the Indian Ocean Dipole (IOD) and El Niño. El Niño sporadically happens in the central Pacific Ocean, characterised by irregular changes in ocean currents and sea surface temperatures (Mukherjee *et al*., 2023). This phenomenon can lead to extreme global weather events like severe droughts, wildfires, heatwaves, destructive floods, and tropical storms (Siqueira *et al*., 2019). In Indonesia, El Niño notably impacts rainfall patterns, causing significant dry spells, particularly during the dry seasons of June-July-August and September-October-November. These dry conditions increase the risk of drought, large-scale forest fires, and haze (Setiawan *et al*., 2017; Supari *et al*., 2018). Strong El Niño events occurred in 1982, 1997, and 2015 due to their high Niño 3.4 index exceeding 2.0 °C (Li *et al*., 2022). The El Niño occurrence in 2023 is classified as a strong event, reaching the threshold of 2.0 °C (Adler, and Gu, 2024). IOD is a global climate phenomenon characterised by anomalies in sea surface temperatures resulting from interactions between the ocean and the atmosphere in the equatorial region of the Indian Ocean (Saji *et al*., 1999). The impact of the IOD on Indonesia generally causes a decrease in average precipitation during the positive phases of the IOD and an increase during the negative phases (Amirudin *et al*., 2020; Kurniadi *et al*., 2021). The most severe droughts typically occur in September, October, and November (SON) (Lestari *et al*., 2018). The IOD in 2019 was noted as the most extreme IOD (Ratna *et al*., 2021; Iskandar *et al*., 2022).

Karawang ranks as the second-largest rice producer in West Java Province. West Java serves as a cornerstone for national food security. Rice production in Karawang amounted to 1,117,814 tons in 2019 and 1,096,657 tons in 2023. Comparatively, production declined by 22,300 tons in 2019 and 43,457 tons in 2023 compared to the average production during the period from 2010 to 2023 (BPS, 2024). This reduction was directly attributed to drought conditions affecting the area (BNPB, 2023).

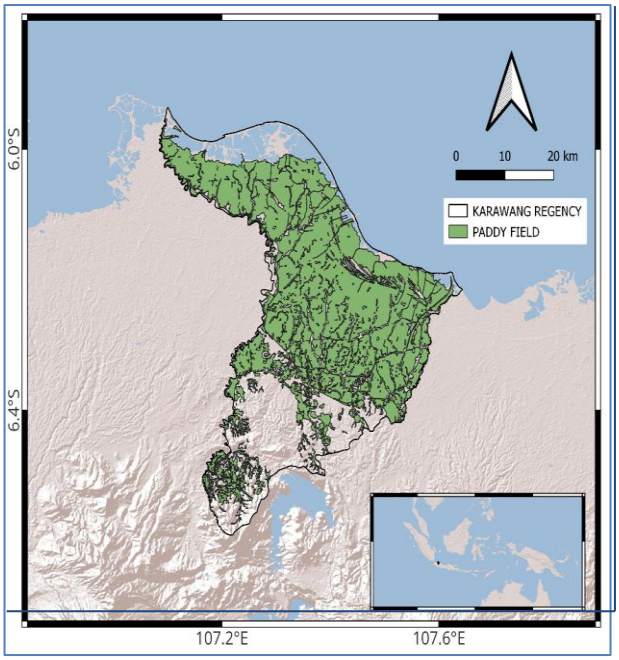

Fig. 1. Research location

Research conducted on drought in Karawang has indicated an exacerbation of drought conditions linked to the El Niño phenomenon in 2015 (Faliha Dzakiyah, and Saraswati, 2020; Dzakiyah *et al*., 2022). Expanding on a broader geographical scope, Dimyati *et al*. (2024) observed similar trends and underscored the significant impact of the IOD on drought, drawing from data from 2001 to 2020. However, no investigation has yet been conducted into the specific ramifications of the 2023 El Niño event on drought in Karawang Regency. This study aims to analyse the effects of the 2023 El Niño compared to the severe IOD event of 2019 on agricultural drought in Karawang Regency.

2. Data and methodology

2.1. *Location of interest*

The research is conducted in the rice paddy fields in Karawang Regency, in the northern West Java Province (Fig. 1). These rice fields span an area of 115,743 hectares, comprising 60% of the total land area of Karawang Regency.

Table 1

The component of composite data

Composite	Imagery Date	Composite	Imagery Date
May-2019	5 May 2019 15 May 2019 20 May 2019 25 May 2019 30 May 2019	May-2023	9 May 2023 14 May 2023 29 May 2023
Jun-2019	9 Jun 2019 19 Jun 2019 24 Jun 2019 29 Jun 2019	Jun-2023	8 Jun 2023 18 Jun 2023 23 Jun 2023 28 Jun 2023
Jul-2019	4 Jul 2019 9 Jul 2019 14 Jul 2019 24 Jul 2019 29 Jul 2019	Jul-2023	3 Jul 2023 13 Jul 2023 18 Jul 2023 23 Jul 2023 28 Jul 2023
Aug-2019	3 Aug 2019 8 Aug 2019 13 Aug 2019 18 Aug 2019 23 Aug 2019 28 Aug 2019	Aug-2023	7 Aug 2023 12 Aug 2023 17 Aug 2023 22 Aug 2023 27 Aug 2023
Sep-2019	2 Sep 2019 12 Sep 2019 22 Sep 2019 27 Sep 2019	Sep-2023	1 Sep 2023 6 Sep 2023 16 Sep 2023 21 Sep 2023 26 Sep 2023
Oct-2019	2 Oct 2019 17 Oct 2019 22 Oct 2019	Oct-2023	6 Oct 2023 11 Oct 2023 16 Oct 2023 21 Oct 2023 26 Oct 2023

2.2. *Data*

We employ multiple datasets, specifically:

(*i*) The Oceanic Niño Index (ONI) utilises data from the Niño 3.4 region in the central equatorial Pacific Ocean to identify active El Niño events, encompassing both conventional strong El Niño and El Niño Modoki phenomena (Ashok *et al*., 2007). To mitigate intraseasonal variability, we employ three-month averages and evaluate El Niño persistence over up to five months. NOAA provides the ONI dataset.

(*ii*) The Indian Ocean Dipole Mode Index is employed to detect negative IOD periods, defined by a threshold of 0.4 °C. This index is sourced from NOAA.

(*iii*) TerraClimate is a dataset providing slightly higher spatial resolution (~4 km) monthly climate and climatic water balance data for global terrestrial surfaces compared to the Climate Hazards Group Infrared Precipitation with Station Data (CHIRPS). It utilises climatically aided interpolation, merging detailed climatological normals from the WorldClim dataset at high spatial resolution with monthly data from other sources at coarser resolutions to generate a monthly precipitation dataset (Abatzoglou *et al*., 2018). TerraClimate has been extensively utilised in drought research by researchers such as Liu *et al*. (2024), Salvacion (2021), Abdi (2019), Chen *et al*. (Chen *et al*., 2024), Lemenkova (2022), Hamarash *et al*. (2022), Gupta *et al*. (Gupta *et al*., 2024), and Venkatappa and Sasaki (2021).

(*iv*) Red, NIR, SWIR, and Green spectral data from Sentinel-2 satellite images, accessed via the Google Earth Engine catalogue, are employed to compute drought indicators. These images depict surface reflectance that has been adjusted for atmospheric effects. Selected images have a maximum cloud cover of 50% and undergo masking procedures. Monthly average pixel values are selected to represent each respective month. Sentinel-2 satellite imagery is preferred over Landsat-8 due to its superior performance in prior research studies (Mallinis *et al*., 2018; Wang *et al*., 2020; Howe *et al*., 2022). The earliest available Sentinel-2 imagery dates back to 2019, with a spatial resolution of 10 meters. Sentinel-2 has an average revisit period of 3.9 days, with a standard deviation of 1.3 days, while Landsat 8/9 has a more extended revisit period of 7.5 days, with a standard deviation of 2.8 days (Jia *et al*., 2024). In Table 1, each composite consists of 3-5 images. Conversely, in other months of 2019 and 2023, only one image was obtained under a maximum of 50% cloud cover.

2.3. *Standardized Precipitation Index*

The Standardized Precipitation Index (SPI) serves as a meteorological drought indicator. SPI utilises a standardisation method to modify accumulated precipitation data across defined periods (timescales) to match an appropriate statistical distribution, typically gamma. It then converts this data into a standard normal distribution. The calculation of SPI follows these procedural steps (Balbo *et al*., 2019; Kourtis *et al*., 2023): The probability density function (PDF) for the gamma distribution is:

$$g(x) = \frac{1}{\beta^{\alpha}\,\gamma(\alpha)}\, x^{\,\alpha-1}\; e^{-x/\beta} \tag{1}$$

where α is a shape parameter ($\alpha > 0$); b is a scale parameter ($\beta > 0$); x is the precipitation value ($x > 0$); and γ (α) is the gamma function, expressed as $\int_0^{\infty} y^{\alpha-1}\, y^{-y}\, dy$. The α and β parameters are assessed as follows:

$$\alpha = \frac{1+\sqrt{1+\frac{4A}{3}}}{4\mathrm{A}};\;\; \beta\,\frac{\bar{x}}{\alpha} \tag{2}$$

TABLE 2

SPI classification.

SPI Value	Category
≤ 2.00	Extremely wet
1.50 to 1.99	Severely wet
1.00 to 1.49	Moderately wet
0 to 0.99	Near normal (mildly wet)
0 to − 0.99	Near normal (mild drought)
-1.00 to −1.49	Moderate drought
-1.50 to −1.99	Severe drought
≥ -2	Extreme drought

where $A = \ln(\overline{x}) - \frac{\sum \ln(x)}{n}$ and n is the number of observations in the time series. A precipitation event has a cumulative probability G (x) given by:

$$G(x) = \int_0^x g(x)dx = \frac{\int_0^x x^{\alpha-1}e^{-x/\beta}\,dt}{\beta^{\alpha}\ \Gamma(\alpha)} \quad (3)$$

By letting t = x/ β, Equation (3) becomes the incomplete gamma function:

$$G(x) = \frac{\int_0^x t^{\alpha-1}e^{-t}\,dt}{\Gamma(\alpha)} \quad (4)$$

Since the gamma distribution is not defined for x = 0, the cumulative probability of zero precipitation (q) is taken into account separately; the final cumulative probability is then calculated using the following formula:

$$H(x) = q + (1-q)G(x) \quad (5)$$

$$SPI = -\left(t - \frac{c_0+c_1+c_2 t^2}{1+d_1 t+d_2 t^2+d_3 t^3}\right); 0 < H(x) \leq 0.5 \quad (6)$$

where $t = \sqrt{\ln(1/H(x)^2}$

$$SPI = t - \frac{c_0+c_1+c_2 t^2}{1+d_1 t+d_2 t^2+d_3 t^3}; 0.5 < H(x) \leq 1 \quad (7)$$

where $t = \sqrt{\ln(1/[1-H(x)^2]}$ and the values of the various constants are $c_0 = 2.515517$ $c_1 = 0.802853$, $c_2 = 0.010328$, $d_1 = 1.43278$ $d_2 = 0.189269$, $d_3 = 0.00138$. The intensity of drought events based on SPI can be classified according to the value of SPI. Table 2 presents the most typical classification.

2.4. *Normalized Difference Drought Index*

The normalized difference drought index (NDDI) is employed as an agricultural drought indicator (Trinh, and Vu, 2019). NDDI is calculated using the normalized difference vegetation index (NDVI) and normalized difference water index (NDWI) inputs. NDVI is computed using the following equation (Townshend, Justice, 1986):

$$NDVI = \frac{NIR-RED}{NIR+RED} \quad (8)$$

The normalized difference water index (NDWI) has undergone various modifications. Initially, NDWI used the following equation (McFeeters, 1996):

$$NDWI = \frac{GREEN - NIR}{GREEN + NIR} \quad (9)$$

In their research, Gu *et al*. (2007) replaced the NDWI calculation by using the NIR and SWIR bands at a wavelength of 2.130 nm. Similarly, Gulácsi and Kovács (2015) utilized the same SWIR channel. The closest Sentinel-2 image channel is SWIR2, with a wavelength of 2202.4 nm (Shang dan Zhu, 2019). Thus, the calculation becomes:

$$NDWI = \frac{NIR-SWIR2}{NIR+SWIR2} \quad (10)$$

The calculation of NDDI follows the equation provided by Gu *et al*. (2007):

$$NDDI = \frac{NDVI-NDWI}{NDVI+NDWI} \quad (11)$$

The NDDI is derived from a normalisation process that scales values between -1 and 1, as outlined by Paniagua *et al*. (2020). Normalisation involves dividing values by the absolute maximum upper or lower fence observed in the boxplot diagram. Upper and lower fence values serve as thresholds for division, ensuring that outlier values are excluded from the calculation. According to Gulácsi and Kovács (2018), outliers are removed during the NDDI computation and replaced with upper or lower fence values. The upper and lower fence (ULF) values are determined based on quartile 3 (Q3) and quartile 1 (Q1), following the formula established by Wilcox (2003).

$$ULF = |Q3 \pm 1.5(Q3 - Q1)| \quad (12)$$

In general, NDDI < 0 is categorised as representing water bodies or no drought, whereas NDDI >= 0 indicates drought conditions (Gulácsi, and Kovács, 2018; Paniagua *et al*., 2020). The classification of NDDI is illustrated in Table 3.

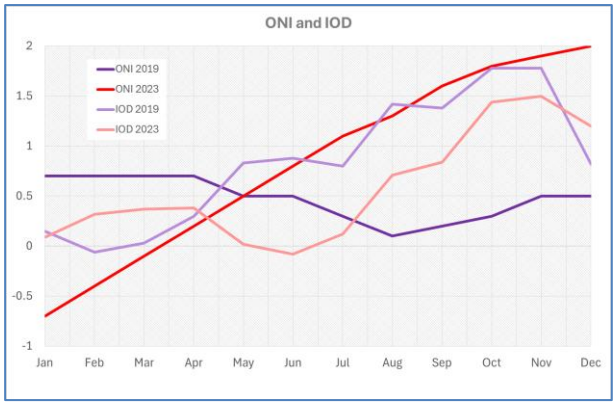

Fig. 2. Oceanic Niño Index (ONI) and Indian Ocean dipole (IOD) mode index

TABLE 3

NDDI Classification

Classification	Value
Water Body/ No Droght	≤0
Low	>0 - 0.33
Moderate	0.33 - 0.66
High	0.66 - 1

3. Results and discussion

3.1. *El Niño and IOD indexes analysis*

Fig. 2 shows ONI 2019 peaked at 0.7 from January to April, indicating active El Niño conditions (red). After July, ONI showed neutral conditions. In contrast, ONI 2023 dropped to -0.7 in January, signaling active La Nina (blue) conditions, transitioning to active El Niño (red) from May onwards, reaching a peak of 2 in December. The high ONI values denote strong El Niño conditions. Compared to 1997 and 2015, ONI in 2023 was lower, whereas ONI in 1997 and 2015 exceeded two and lasted longer, as noted by Adler and Gu (2024).

Regarding the IOD phenomenon, the index in 2019 was positive >0.4 (red) from May to December, with the maximum index reaching 1.78 in October and November. Ratna *et al*. (2021) and Iskandar *et al*. (2022) referred to this as an extreme IOD event. The IOD in 2019 was among the highest, comparable only to those in 1994 and 1997 (Doi *et al*., 2020). The magnitude of the IOD in 2019 was due to a very large interhemispheric pressure gradient between the South China Sea and the Australian continent (Lu, and Ren, 2020). Furthermore, the 2019 IOD was independent as it did not coincide with El Niño (Kurniadi *et al*., 2021). In 2023, positive IOD >0.4 (red) occurred from August to December, with the highest value of 1.44 in October.

3.2. *Meteorological Drought Analysis*

Figs. 3(d-e) and 3(j-k) show that the most severe meteorological droughts occurred in August and September, reaching severe levels in 2019 and 2023. The severe drought in 2023 was more extensive than in 2019, attributable to the impacts of elevated IOD and ONI indices. In June-July Figs. 3(a-b), severe drought was only evident in 2019. Conversely, for October (Figs. 3f and 3l), moderate drought was observed only in 2023. The drought phase 2023 lagged behind 2019, as the IOD index exceeded 0.4 earlier in May 2019, whereas ONI >0.5 occurred in June. There is also an approximate 2-month lag between the onset of severe drought and the activation of IOD and active El Niño.

Comparing the meteorological droughts of 2023 and 2019, the May-July 2019 drought Figs. 4(a-c) was more pronounced than in 2023, indicated by a positive SPI difference with the highest value in July. Conversely, from August to October Figs. 4(d-f), drought in 2023 was more severe than in 2019, marked by a negative SPI difference with the lowest value in October. These patterns resulted from differences in the drought phases (Figure 3), where the 2019 drought phase preceded that of 2023.

3.3. *Agricultural Drought Analysis*

In the boxplot diagram (Fig. 5), the spatial range of NDDI in August 2019 was the widest, while May 2019 exhibited the narrowest range based on upper and lower fence values. The spatial range of data in 2019 was more extensive than in 2023, as evidenced by higher upper fence values and lower fence values, except for May, September, and October. The highest upper fence value recorded was 1.39, and the lowest lower fence was -1.78, making 1.78 the normalization divider for classifying NDDI.

Low drought conditions were predominant in May 2019 (Fig. 6a). Conversely, in May 2023, low drought was only observed in the western and southern regions (Fig. 6g). A significant expansion of drought occurred in the northern and central parts in June 2019 (Fig. 6b). June 2019 generally showed water body/no drought conditions, with moderate drought observed in small portions in the north, central, and south. This differs from the findings of Dzakiyah *et al*. (2022), where low drought predominated in the Ciampel District. Only low drought was predominant in the same area in June 2023 (Fig. 6h). In July 2023, low drought was predominant, with moderate and high drought occurring in small parts (Fig. 6i). In August 2019 (Fig. 6d), moderate and high drought persisted in small areas in the north and central regions.

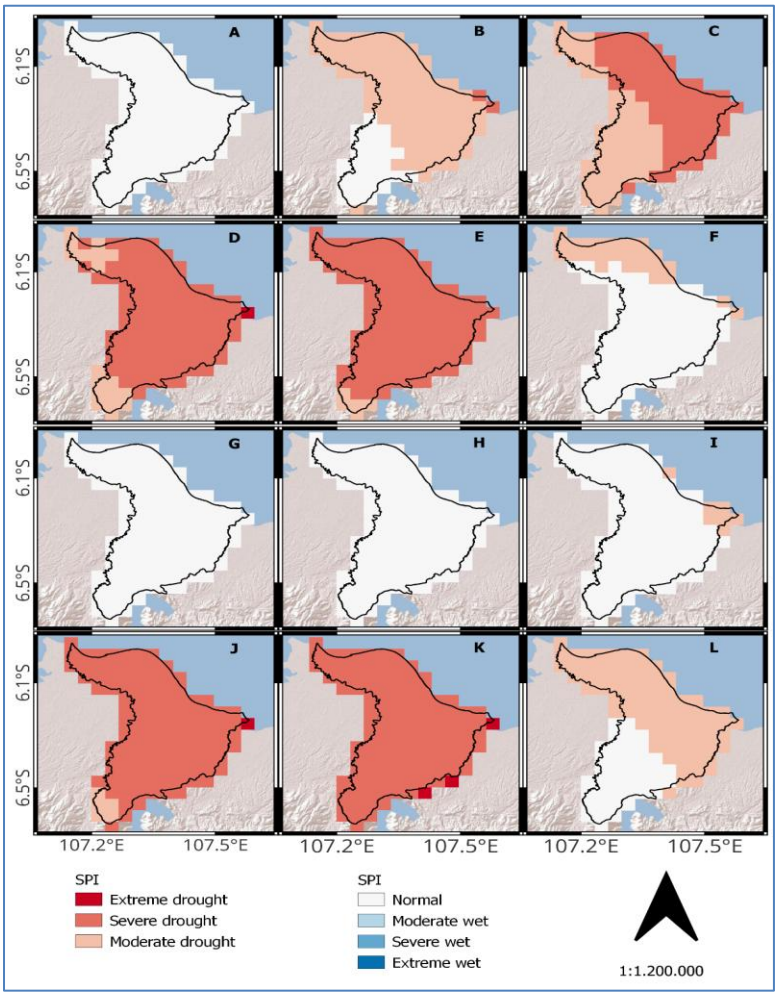

Figs. 3(a-l). SPI in a) May, b) June, c) July, d) August, e) September, and f) October 2019. (g-l) are for 2023

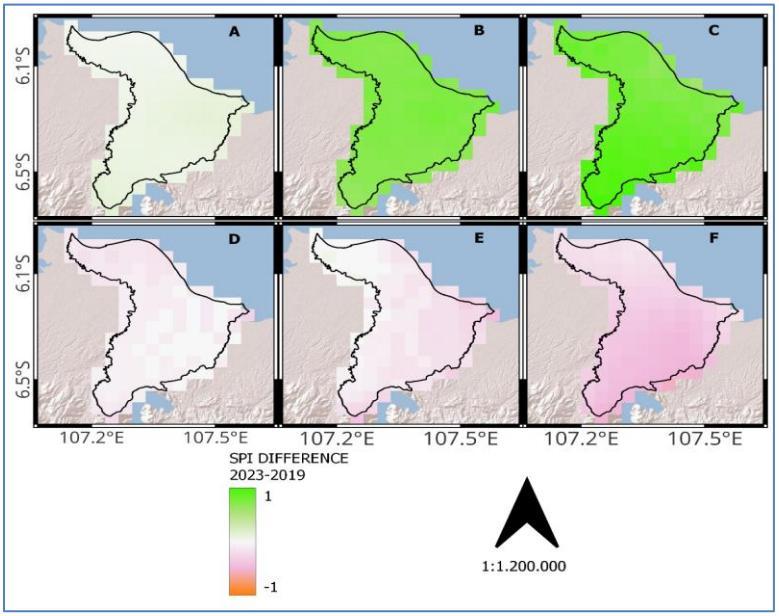

Figs. 4(a-f). SPI difference between 2023 and 2019 for a) May, b) June, c) July, d) August, e) September, and f) October.

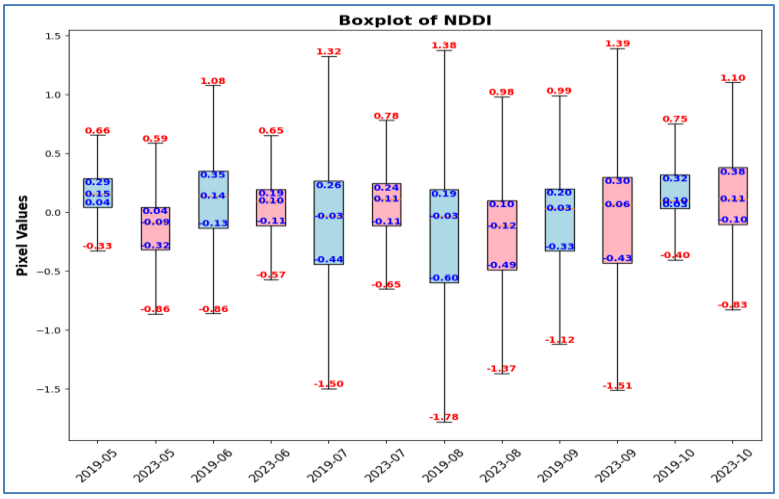

Fig. 5. Boxplot of NDDI spatial distribution

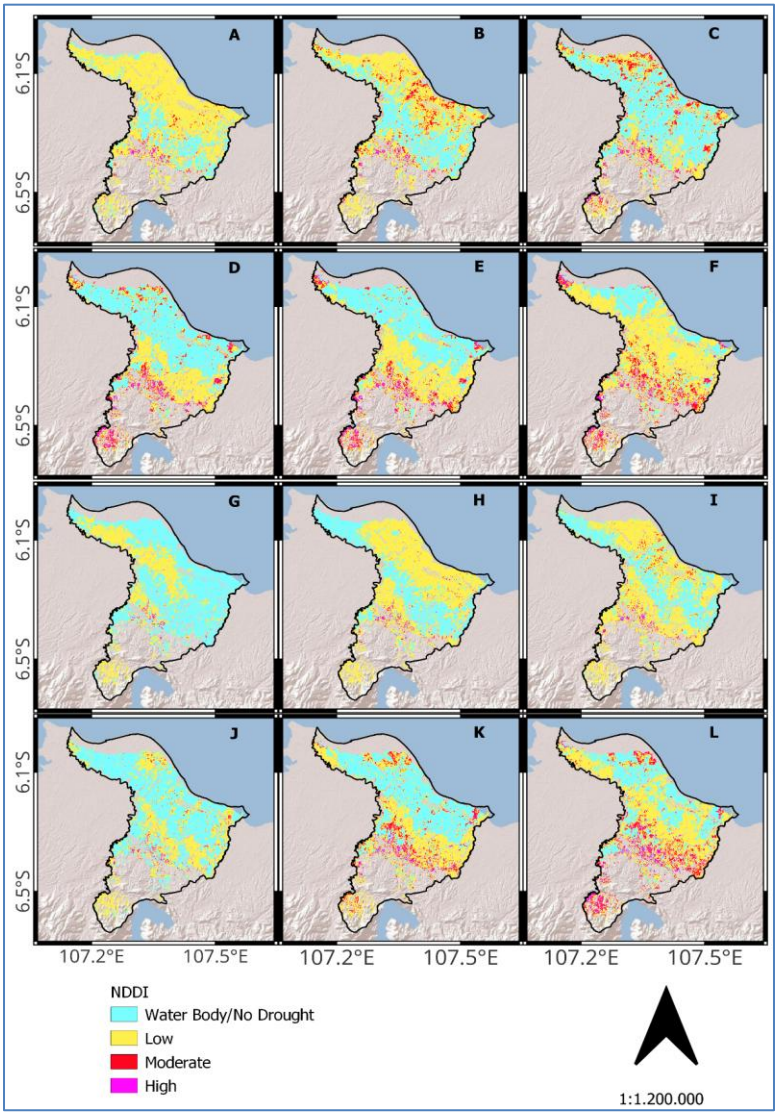

Figs. 6(a-l). NDDI in a) May, b) June, c) July, d) August, e) September, and f) October 2019. (g-l) are for 2023

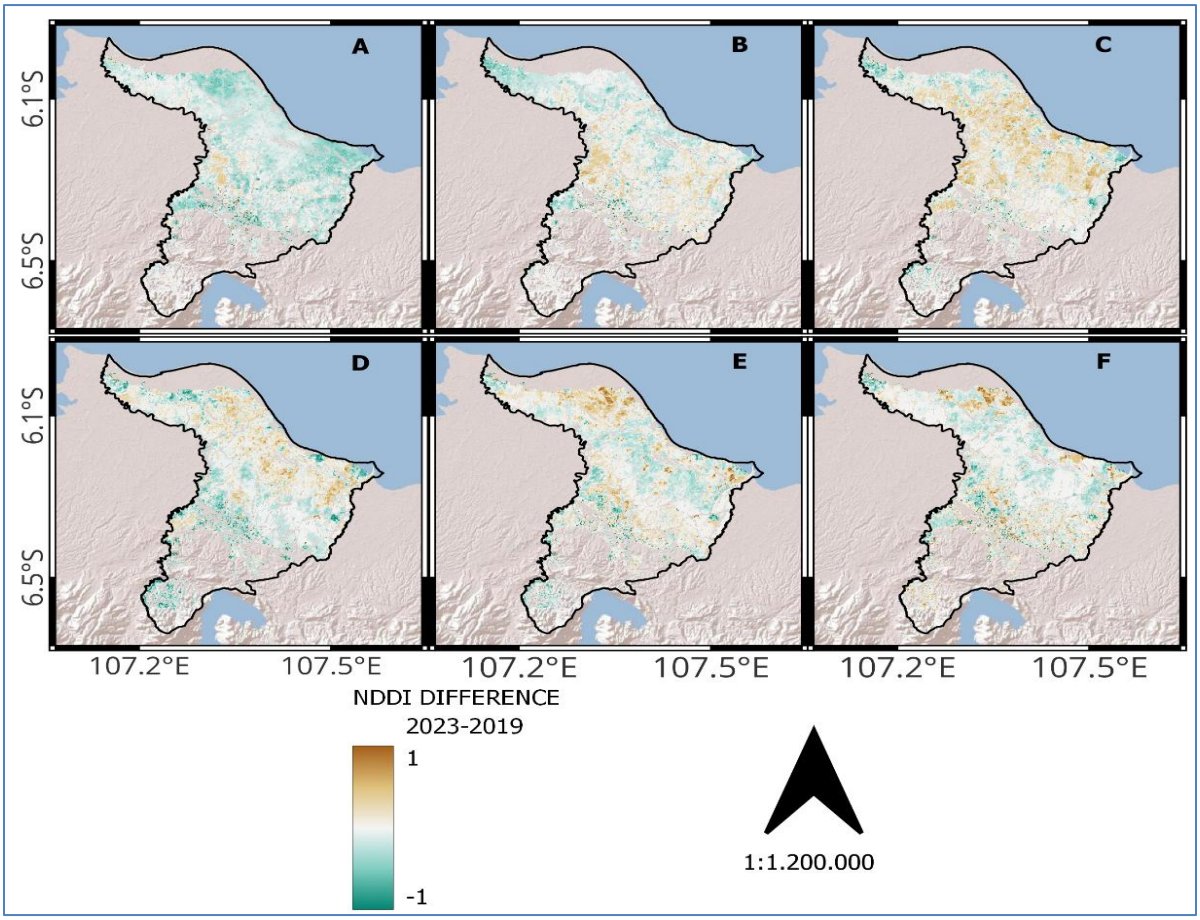

Figs. 7(a-f). NDDI difference between 2023 and 2019 for a) May, b) June, c) July, d) August, e) September, and f) October

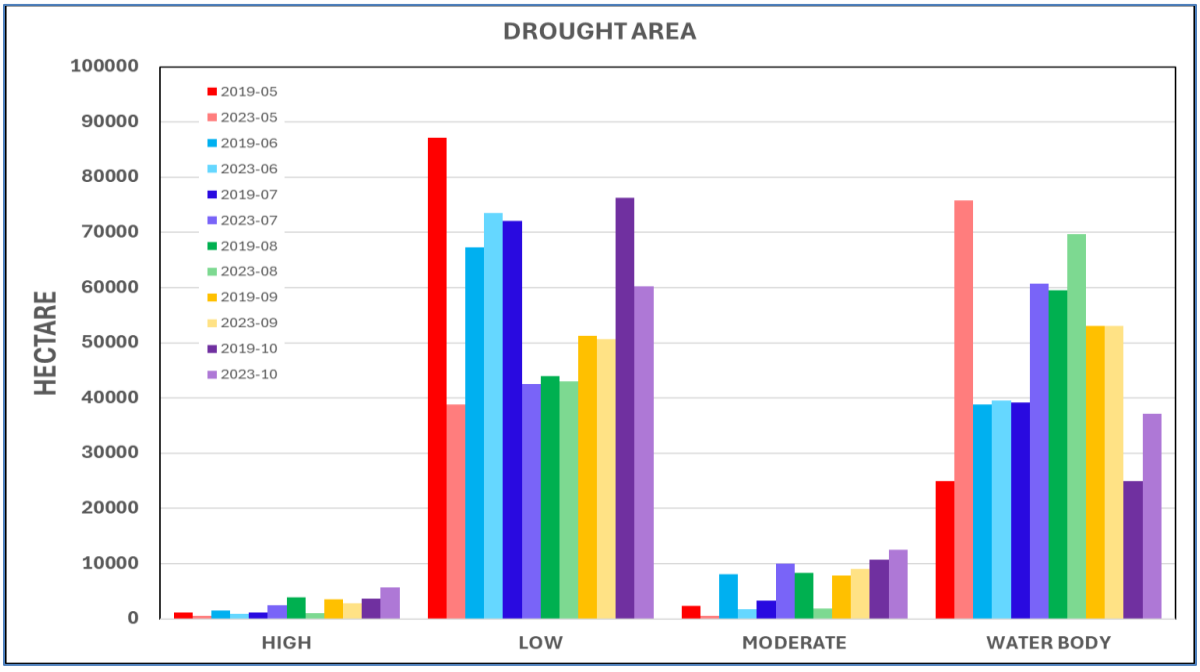

Fig. 8. Graphic of the drought area in 2019 and 2023

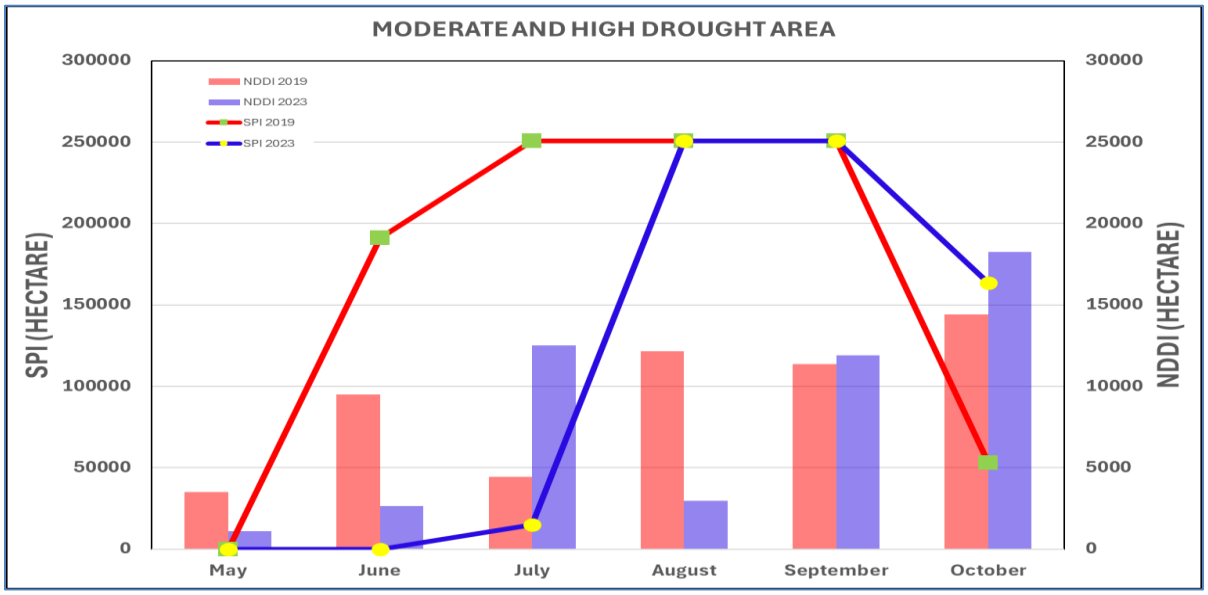

Fig. 9. Moderate and high drought areas based on NDDI and SPI in 2019 and 2023.

In contrast, low drought was predominant in August 2023 (Fig. 6j). Moderate and high drought in the northern areas transitioned to water body/no drought conditions in September 2019 (Fig. 6e). Meanwhile, moderate and high drought replaced water body/no drought in the north and emerged in the central and southern regions in September 2023 (Fig. 6k). Moderate and high drought in October 2023 (Fig. 6l) was more extensive than in October 2019, particularly in the central region (Fig. 6f).

Drought in May and June 2019 was more severe compared to 2023 Fig. 7(a-b). Conversely, drought in July 2023 was higher than in 2019, indicated by positive values in Fig. 7c, though it only reached low levels. Generally, drought from August to October 2019 was more extensive than in 2023 Fig. 7(c-e). Still, positive values appeared in the northern and some central regions, depicting greater drought severity in those areas in 2023.

Fig. 8 illustrates a broader expanse of water bodies or absence of drought in 2023, averaging 52,933 hectares, compared to a mere 37,778 hectares in 2019. Conversely, the extents of low (67,709 Ha), moderate (7,253 Ha), and high drought (2,914 Ha) in 2019 surpassed those in 2023, with areas measuring 54,756 Ha, 5,668 Ha, and 2,297 Ha, respectively, for low, moderate, and high drought levels. Moderate drought in 2023 was more extensive in July, September, and October compared to 2019, except for May, June, and August. The high drought in 2023 exceeded 2019 only in July and October.

In Fig. 9, the comparison of moderate and high levels of meteorological and agricultural droughts indicates a peak delay of three months in 2019 and two months in 2023. This delay can be attributed to the soil's capacity to retain water, which mitigates immediate desiccation following a reduction in rainfall (Ma'rufah *et al*., 2017; Tian *et al*., 2022; Xu *et al*., 2023). In both October 2019 and 2023, agricultural drought reached its peak while meteorological drought experienced a decline. However, reductions were observed in July 2019 and August 2023. The decrease in drought severity may be associated with water management practices implemented through irrigation channels from the Jatiluhur Reservoir, which are essential for rice cultivation in Karawang (Dimyati *et al*., 2024).

4. Conclusions

El Niño and the Indian Ocean Dipole (IOD) are climatic phenomena that induce periods of drought. In 2019, there was a notably strong positive IOD event, while in 2023, a significant El Niño event coincided with a positive IOD phase. The most severe meteorological droughts occurred in August and September of both 2019 and 2023, with the 2023 drought being more extensive due to elevated IOD and ONI indices. There was an approximate two-month lag between the onset of severe meteorological drought and the manifestation of the IOD and El Niño phenomena. From 2019 to 2023, agricultural drought exhibited substantial fluctuations across various months and regions. In 2019, May and June experienced more widespread and severe drought, particularly in northern and central areas, compared to 2023. However, by July and subsequent months, 2023 witnessed higher drought severity in certain regions than in 2019, indicating

significant variations in drought extent and intensity during the study period. According to agricultural drought classifications, moderate drought in 2023 (2019) was more prevalent in July, September, and October (May, June, and August). The high-level agricultural drought in 2023 (2019) was more intense in July and October (May, June, August, and September). There was a gap of about two (three) months between the onset of meteorological drought and agricultural drought in 2019 (2023), likely attributable to differences in soil water retention capacities. The agricultural drought reached its peak in October 2019 (2023), after experiencing a decrease in July (August). This decrease was impacted by water management practices through irrigation channels originating from the Jatiluhur Reservoir.

Acknowledgments

The authors would like to acknowledge the head of the research center of limnology and water resources, Dr. Boedi Tjahjono and Mrs. Rizqi Ianatus from IPB University for valuable discussion.

Conflicts of Interest. The authors reported no potential conflicts of interest.

Authors' Contribution.

AFR was the first author who conceived and designed the analysis, collected the data, performed the analysis, and wrote the paper. MMS and A were the co-authors who compiled the data and performed the analysis.

References

Abatzoglou, J. T., Dobrowski, S. Z., Parks, S. A., Hegewisch, K. C., 2018, "TerraClimate, a high-resolution global dataset of monthly climate and climatic water balance from 1958-2015", Scientific Data, 5, 1–12. https://doi.org/10.1038/sdata.2017.191

Abdi, O., 2019, "Climate-triggered insect defoliators and forest fires using multitemporal landsat and terraclimate data in NE Iran: An application of GEOBIA treenet and panel data analysis", Sensors (Switzerland), 19, 18. https://doi.org/10.3390/s19183965

Adler, R. F., Gu, G., 2024, "Global Precipitation for the Year 2023 and How It Relates to Longer Term Variations and Trends", Atmosphere, 15, 5, 535. https://doi.org/10.3390/atmos15050535

American Meteorological Society, 2019, "Drought", . https://www.ametsoc.org/index.cfm/ams/about-ams/ams-statements/archive-statements-of-the-ams/drought/, accessed 19June2024

Amirudin, A. A., Salimun, E., Tangang, F., Juneng, L., Zuhairi, M., 2020, "Differential influences of teleconnections from the Indian and Pacific oceans on rainfall variability in Southeast Asia", Atmosphere, 11, 9, 13–15. https://doi.org/10.3390/ATMOS11090886

Ashok, K., Behera, S. K., Rao, S. A., Weng, H., Yamagata, T., 2007, "El Niño Modoki and its possible teleconnection", Journal of Geophysical Research: Oceans, 112, 11. https://doi.org/10.1029/2006JC003798

Balbo, F., Wulandari, R. A., Nugraha, M. R. R., Dwiandani, A., Syahputra, M. R., Suwarman, R., 2019, "The evaluation of drought indices: Standard Precipitation Index, Standard Precipitation Evapotranspiration Index, and Palmer Drought Severity Index in Cilacap-Central Java", IOP Conference Series: Earth and Environmental Science, 303, 1. https://doi.org/10.1088/1755-1315/303/1/012012

BNPB, 2023, "Kekeringan Pulau Jawa", . https://data.bnpb.go.id/pages/kekeringan-pulau-jawa, accessed 19June2024

BPS, 2024, "Produksi Padi Menurut Kabupaten/Kota (Ton)", . https://jabar.bps.go.id/indicator/53/52/1/produksi-padi-menurut-kabupaten-kota.html, accessed 19June2024

Chen, Y., Taylor, P., Cuddy, S., Wahid, S., Penton, D., Karim, F., 2024, "Inferring vegetation response to drought at multiscale from long-term satellite imagery and meteorological data in Afghanistan", Ecological Indicators, 158. https://doi.org/10.1016/j.ecolind.2024.111567

Dimyati, M., Rustanto, A., Ash Shidiq, I. P., Indratmoko, S., Siswanto, Dimyati, R. D., Nurlambang, T., Zubair, A., Fakhruddin, A., Siddiq, A., Adhanto, D. H., Maulidina, K., Auni, R., 2024, "Spatiotemporal relation of satellite-based meteorological to agricultural drought in the downstream Citarum watershed, Indonesia", Environmental and Sustainability Indicators, 22. https://doi.org/10.1016/j.indic.2024.100339

Doi, T., Behera, S. K., Yamagata, T., 2020, "Predictability of the Super IOD Event in 2019 and Its Link With El Niño Modoki", Geophysical Research Letters, 47, 7, 1–9. https://doi.org/10.1029/2019GL086713

Dzakiyah, I. F., Saraswati, R., Pamungkas, F. D., 2022, "The Potential of Agricultural Land Drought Using Normalized Difference Drought Index in Ciampel Subdistrict Karawang Regency", International Journal on Advanced Science, Engineering and Information Technology, 12, 3, 908–914. https://doi.org/10.18517/ijaseit.12.3.13261

Faliha Dzakiyah, I., Saraswati, R., 2020, "Drought area of agricultural land using Tasseled Cap Transformation (TCT) method in Ciampel Subdistrict Karawang Regency", E3S Web of Conferences, 211, 1–10. https://doi.org/10.1051/e3sconf/202021102005

Farmlands, W., Wang, Q., Li, J., Jin, T., Chang, X., Zhu, Y., Li, Y., Sun, J., Li, D., 2020, "Comparative Analysis of Landsat-8, Sentinel-2, and GF-1 Data for Retrieving Soil Moisture over Wheat Farmlands", Remote Sensing, 1, 17. https://doi.org/10.3390/RS12172708

Gu, Y., Brown, J. F., Verdin, J. P., Wardlow, B., 2007, "A five-year analysis of MODIS NDVI and NDWI for grassland drought assessment over the central Great Plains of the United States", Geophysical Research Letters, 34, 6. https://doi.org/10.1029/2006GL029127

Gulácsi, A., Kovács, F., 2015, "Drought Monitoring With Spectral Indices Calculated From Modis Satellite Images In Hungary", Journal of Environmental Geography, 8, 3–4, 11–20. https://doi.org/10.1515/jengeo-2015-0008

Gulácsi, A., Kovács, F., 2018, "Drought monitoring of forest vegetation using MODIS-based normalized difference drought index in Hungary", Hungarian Geographical Bulletin, 67, 1. https://doi.org/10.15201/hungeobull.67.1.3

Gupta, A., Jain, M. K., Pandey, R. P., Gupta, V., Saha, A., 2024, "Evaluation of global precipitation products for meteorological drought assessment with respect to IMD station datasets over India", Atmospheric Research, 297. https://doi.org/10.1016/j.atmosres.2023.107104

Hamarash, H., Hamad, R., Rasul, A., 2022, "Meteorological drought in semi-arid regions: A case study of Iran", Journal of Arid Land, 14, 11. https://doi.org/10.1007/s40333-022-0106-9

Howe, A. A., Parks, S. A., Harvey, B. J., Saberi, S. J., Lutz, J. A., Yocom, L. L., 2022, "Comparing Sentinel-2 and Landsat 8 for Burn Severity Mapping in Western North America", Remote Sensing, 14, 20, 1–21. https://doi.org/10.3390/rs14205249

Iskandar, I., Lestari, D. O., Saputra, A. D., Setiawan, R. Y., Wirasatriya, A., Susanto, R. D., Mardiansyah, W., Irfan, M., Rozirwan, Setiawan, J. D., Kunarso, 2022, "Extreme Positive Indian Ocean Dipole in 2019 and Its Impact on Indonesia", Sustainability (Switzerland), 14, 22, 1–15. https://doi.org/10.3390/su142215155

Jia, K., Hasan, U., Jiang, H., Qin, B., Chen, S., Li, D., Wang, C., Deng, Y., Shen, J., 2024, "How frequent the Landsat 8/9-Sentinel 2A/B virtual constellation observed the earth for continuous time series monitoring", International Journal of Applied Earth Observation and Geoinformation, 130, December 2023, 103899. https://doi.org/10.1016/j.jag.2024.103899https://doi.org/10.1016/j.jag.2024.103899

Kourtis, I. M., Vangelis, H., Tigkas, D., Mamara, A., Nalbantis, I., Tsakiris, G., Tsihrintzis, V. A., 2023, "Drought Assessment in Greece Using SPI and ERA5 Climate Reanalysis Data", Sustainability (Switzerland) , 15, 22, 1–19. https://doi.org/10.3390/su152215999

Kurniadi, A., Weller, E., Min, S. K., Seong, M. G., 2021, "Independent ENSO and IOD impacts on rainfall extremes over Indonesia", International Journal of Climatology, 41, 6. https://doi.org/10.1002/joc.7040

Lemenkova, P., 2022, "Mapping Climate Parameters over the Territory of Botswana Using GMT and Gridded Surface Data from TerraClimate", ISPRS International Journal of Geo-Information, 11, 9. https://doi.org/10.3390/ijgi11090473

Lestari, D. O., Sutriyono, E., Sabaruddin, S., Iskandar, I., 2018, "Respective Influences of Indian Ocean Dipole and El Niño-Southern Oscillation on Indonesian Precipitation", Journal of Mathematical and Fundamental Sciences, 50, 3, 257–272. https://doi.org/10.5614/j.math.fund.sci.2018.50.3.3

Li, L., Chen, X., Li, C., Li, X., Yang, M., 2022, "Comparison of Madden-Julian oscillation in three super El Niño events", Frontiers in Earth Science, 10, February, 1–11. https://doi.org/10.3389/feart.2022.1021953

Liu, M., Trugman, A. T., Peñuelas, J., Anderegg, W. R. L., 2024, "Climate-driven disturbances amplify forest drought sensitivity", Nature Climate Change. https://doi.org/10.1038/s41558-024-02022-1

Lu, B., Ren, H. L., 2020, "What Caused the Extreme Indian Ocean Dipole Event in 2019?", Geophysical Research Letters, 47, 11, 1–8. https://doi.org/10.1029/2020GL087768

Ma'rufah, U., Hidayat, R., Prasasti, I., 2017, "Analysis of relationship between meteorological and agricultural drought using standardized precipitation index and vegetation health index", Journal of Physics: Conference Series, 755, 1. https://doi.org/10.1088/1755-1315/54/1/012008

Mallinis, G., Mitsopoulos, I., Chrysafi, I., 2018, "Evaluating and comparing sentinel 2A and landsat-8 operational land imager (OLI) spectral indices for estimating fire severity in a mediterranean pine ecosystem of Greece", GIScience and Remote Sensing, 55, 1, 1–18. https://doi.org/10.1080/15481603.2017.1354803

McFeeters, S. K., 1996, "The use of the Normalized Difference Water Index (NDWI) in the delineation of open water features", Remote Sensing of Environment, 25, 3, 687–711. https://doi.org/10.1016/S0034-4257(96)00038-7

Mishra, A. K., Singh, V. P., 2010, "A review of drought concepts", Journal of Hydrology, 391, 1–2. https://doi.org/10.1016/j.jhydrol.2010.07.012

Mukherjee, S., Pal, J., Manna, S., Saha, A., Das, D., 2023, "El-Niño Southern Oscillation and its effects", Visualization Techniques for Climate Change with Machine Learning and Artificial Intelligence. https://doi.org/10.1016/b978-0-323-99714-0.00013-3

Paniagua, M. T., Villalba, J., Pasten, M., 2020, "Spatial-temporal distribution of drought in the western region of paraguay (2005-2017)", International Archives of the Photogrammetry, Remote Sensing and Spatial Information Sciences - ISPRS Archives, 42, 3/W12, 327–330. https://doi.org/10.5194/isprs-archives-XLII-3-W12-2020-327-2020

Ratna, S. B., Cherchi, A., Osborn, T. J., Joshi, M., Uppara, U., 2021, "The Extreme Positive Indian Ocean Dipole of 2019 and Associated Indian Summer Monsoon Rainfall Response", Geophysical Research Letters, 48, 2, 1–11. https://doi.org/10.1029/2020GL091497

Saji, N. H., Goswami, B. N., Vinayachandran, P. N., Yamagata, T., 1999, "A dipole mode in the tropical Indian ocean", Nature, 401, 6751. https://doi.org/10.1038/43854

Salvacion, A. R., 2021, "Mapping meteorological drought hazard in the Philippines using SPI and SPEI", Spatial Information Research, 29, 6. https://doi.org/10.1007/s41324-021-00402-9

Setiawan, A. M., Lee, W. S., Rhee, J., 2017, "Spatio-temporal characteristics of Indonesian drought related to El Niño events and its predictability using the multi-model ensemble", International Journal of Climatology, 37, 13. https://doi.org/10.1002/joc.5117

Siqueira, L., Ramírez, E., Camayo, R., 2019, "An Overview of the El Niño, La Niña, and the Southern Oscillation Phenomena: Theory, Observations, and Modeling Links", Towards Mathematics, Computers and Environment: A Disasters Perspective. https://doi.org/10.1007/978-3-030-21205-6_1

Supari, Tangang, F., Salimun, E., Aldrian, E., Sopaheluwakan, A., Juneng, L., 2018, "ENSO modulation of seasonal rainfall and extremes in Indonesia", Climate Dynamics, 51, 7–8. https://doi.org/10.1007/s00382-017-4028-8

Tian, Q., Lu, J., Chen, X., 2022, "A novel comprehensive agricultural drought index reflecting time lag of soil moisture to meteorology: A case study in the Yangtze River basin, China", Catena, 209, P1, 105804. https://doi.org/10.1016/j.catena.2021.105804

Townshend, J. R. G., Justice, C. O., 1986, "Analysis of the dynamics of african vegetation using the normalized difference vegetation index", International Journal of Remote Sensing, 7, 11. https://doi.org/10.1080/01431168608948946

Trinh, L. H., Vu, D. T., 2019, "Application of remote sensing technique for drought assessment based on normalized difference drought index, a case study of Bac Binh district, Binh Thuan province (Vietnam)", Russian Journal of Earth Sciences, 19, 2. https://doi.org/10.2205/2018ES000647

Venkatappa, M., Sasaki, N., 2021, "Datasets of drought and flood impact on croplands in Southeast Asia from 1980 to 2019", Data in Brief, 38. https://doi.org/10.1016/j.dib.2021.107406

Wilcox, R. R., 2003, "Summarizing Data", Applying Contemporary Statistical Techniques, 55–91. https://doi.org/10.1016/B978-012751541-0/50024-9

Wilhite, D. A., Glantz, M. H., 1985, "Understanding: The drought phenomenon: The role of definitions", Water International, 10,

3. https://doi.org/10.1080/02508068508686328

Xu, Z., Wu, Z., Shao, Q., He, H., Guo, X., 2023, "From meteorological to agricultural drought: Propagation time and probabilistic linkages", Journal of Hydrology: Regional Studies, 46, January, 101329. https://doi.org/10.1016/j.ejrh.2023.101329.https://doi.org/10.1016/j.ejrh.2023.101329.